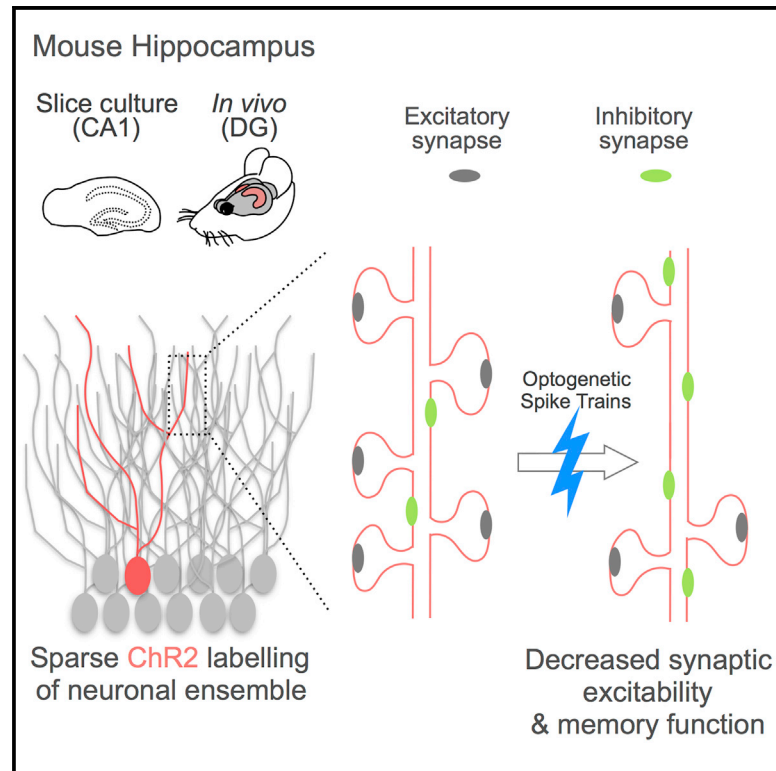


Homeostatic Plasticity in the Hippocampus Facilitates Memory Extinction

Graphical Abstract



Authors

Pablo Mendez, Thomas Stefanelli, Carmen E. Flores, Dominique Muller, Christian Lüscher

Correspondence

pmendez@cajal.csic.es

In Brief

Mendez et al. show that homeostatic synaptic adaptations induced by optogenetic spike trains regulate the function of memory-bearing hippocampal neuronal ensembles.

Highlights

- Optogenetic spike trains are uncoupled from synaptic input in hippocampal neurons
- Dendritic spine formation is reduced via L-type VDCC activity and protein synthesis
- Reducing synaptic excitability in the cellular engram facilitates memory extinction



Homeostatic Plasticity in the Hippocampus Facilitates Memory Extinction

Pablo Mendez,^{1,3,5,*} Thomas Stefanelli,¹ Carmen E. Flores,¹ Dominique Muller,^{1,4} and Christian Lüscher^{1,2}

¹Department of Basic Neurosciences, Faculty of Medicine, University of Geneva, Michel-Servet 1, 1211 Geneva, Switzerland

²Service of Neurology, Geneva University Hospital, Perret-Gentil 4, 1211 Geneva, Switzerland

³Present address: Cajal Institute (CSIC), Av. Dr. Arce 37, 28002 Madrid, Spain

⁴Deceased April 29, 2015

⁵Lead Contact

*Correspondence: pmendez@cajal.csic.es

<https://doi.org/10.1016/j.celrep.2018.01.025>

SUMMARY

Correlated activity in the hippocampus drives synaptic plasticity that is necessary for the recruitment of neuronal ensembles underlying fear memory. Sustained neural activity, on the other hand, may trigger homeostatic adaptations. However, whether homeostatic plasticity affects memory function remains unknown. Here, we use optogenetics to induce cell autonomous homeostatic plasticity in CA1 pyramidal neurons and granule cells of the hippocampus. High-frequency spike trains applied for 10 min decreased the number of excitatory spine synapses and increased the number of inhibitory shaft synapses. This activity stopped dendritic spine formation via L-type voltage-dependent calcium channel activity and protein synthesis. Applied selectively to the ensemble of granule cells encoding a contextual fear memory, the spike trains impaired memory recall and facilitated extinction. Our results indicate that homeostatic plasticity triggered by optogenetic neuronal firing alters the balance between excitation and inhibition in favor of memory extinction.

INTRODUCTION

Potentiation of excitatory transmission, such as long-term potentiation (LTP), believed to underlie many forms of learning and memory, is eventually reset by non-Hebbian forms of plasticity in the interest of long-term network stability (Abbott and Nelson, 2000). Homeostatic and experience-dependent plasticities are calcium dependent (Vitureira et al., 2012), use receptor distribution as expression mechanism (Turrigiano and Nelson, 2004), and are associated with structural remodeling of excitatory (Zuo et al., 2005) and inhibitory synapses (van Versendaal et al., 2012). In the present study, we investigated the role of homeostatic plasticity in memory function.

Ensembles of neurons recruited during memory formation are a “bona fide” substrate for the memory engram. Hebbian forms of synaptic plasticity support the formation of neuronal ensembles, thus contributing to encoding, consolidation, and expression of memory (Gruart et al., 2006). This has been experimen-

tally demonstrated in the case of contextual fear conditioning (CFC) (Josselyn et al., 2015; Tonegawa et al., 2015), where potentiation of excitatory synapses occurs specifically in neurons of the dentate gyrus that express the immediate early gene cFos marking the memory ensemble (Ryan et al., 2015). LTP and long-term depression (LTD) may bidirectionally modulate fear memory expression by acting on ensembles of neurons coding for the conditioned and unconditioned stimuli (CS-US) association in the amygdala (Nabavi et al., 2014). Whereas much evidence supports a causal role for Hebbian forms of plasticity in recruiting neuronal ensembles for contextual fear memory, it remains elusive whether and how homeostatic synaptic plasticity affects memory processes.

With repetitive CS presentation that is not followed by the US, the association is lost, a process referred to as extinction (Herry et al., 2010). Some models propose that extinction constitutes a form of re-learning that creates a new memory trace to counteract the fear memory, but the cellular mechanisms at play remain poorly understood (Myers and Davis, 2007; Maren, 2011). Here, we provide evidence that homeostatic synaptic plasticity in the neuronal ensemble promotes fear extinction. This may not only be relevant for the neuronal mechanisms of extinction but also provides a strategy to facilitate the attenuation of traumatic memories.

Homeostatic synaptic plasticity can adjust neuronal firing rates (Hengen et al., 2016). For example, chronic low-frequency spiking results in non-Hebbian decrease of synaptic strength via glutamate receptor redistribution (Goold and Nicoll, 2010) and changes in axon initial segment excitability (Grubb and Burrone, 2010). Homeostatic adaptations control the strength and structure of γ -amino butyric acid (GABA) synapses onto hippocampal CA1 principal neurons (Flores et al., 2015). Calcium (through Ca^{2+} /calmodulin-dependent protein kinase II [CamKII]) and protein synthesis orchestrate homeostatic synaptic adaptations (Marsden et al., 2010; Petrini et al., 2014; Flores et al., 2015; Goold and Nicoll, 2010).

Structural synaptic plasticity is a core mechanism of homeostatic plasticity (Holtmaat and Svoboda, 2009). The continuous formation and elimination of excitatory and inhibitory synapses participates in the compensatory adaptations to hippocampal network activity changes (De Roo et al., 2008a; Bloodgood et al., 2013). Interestingly, many examples of structural remodeling described to date represent Hebbian forms of plasticity of excitatory synapses and are critically involved in learning, memory



formation (Caroni et al., 2012), and extinction (Lai et al., 2012). It is thus possible that homeostatic plasticity participates in memory processes through the regulation of synaptic structure.

Here, we used firing frequencies naturally attained by hippocampal neurons *in vivo* to study cell-autonomous synaptic consequences of brief episodes of elevated neuronal activity in CA1 neurons *in vitro* and granule cells *in vivo*. We found that, 24 hr after a brief period of optogenetically induced high-frequency spiking activity (spike trains), both types of hippocampal neurons undergo long-term homeostatic adaptations that reduce synaptic excitability by increasing the number of inhibitory while reducing the number of excitatory synapses. We tested the functional consequences of these homeostatic adaptations in granule cells coding for contextual fear memories and observed facilitated memory extinction. Our results indicate that activity can trigger a cell-autonomous homeostatic decrease in synaptic excitability that regulates the function of hippocampal neurons of the memory engram.

RESULTS

Optogenetically Induced Spike Trains Differentially Regulate Excitatory and Inhibitory Synapse Function in CA1 Pyramidal Neurons

We sparsely expressed channelrhodopsin 2 (ChR2-EYFP+mRFP; Figure 1A) in CA1 pyramidal neurons of hippocampal organotypic slice cultures and used the focused light of a blue light-emitting diode (LED) (470 nm) to drive activity of a ChR2-expressing neuron (5 pulses at 10 Hz every second during 10 min; Figure 1B). This firing frequency was chosen to mimic typical firing rates of cells inside its place fields (Harvey et al., 2009; Epsztein et al., 2011; Leutgeb et al., 2005). 24 hr later, we assessed intrinsic and synaptic excitability.

We recorded excitatory and inhibitory miniature postsynaptic currents (mEPSCs and mIPSCs) and found opposite changes. The inter-event interval (IEI) of mEPSCs increased (Figure 1C) whereas that of mIPSC decreased 24 hr after spike trains (Figure 1D) without affecting the amplitude of the recorded mPSCs, excitatory or inhibitory (Figures 1C and 1D). We analyzed the effects of spike trains on intrinsic excitability of the stimulated neurons. Spike trains induced no changes in membrane resting potential, membrane resistance, or input/output curves of stimulated neurons, suggesting unaltered neuronal intrinsic excitability (Figure S1).

To assess alterations in excitation/inhibition (E/I) balance of synaptic inputs, we simultaneously recorded evoked excitatory and inhibitory PSCs (eEPSCs and eIPSCs). The ratio eEPSCs/eIPSCs was reduced 24 hr after spike trains (Figure 1E). These results suggest that optogenetically induced spike trains delivered in organotypic slice cultures decrease excitatory but increase inhibitory synaptic currents, thereby reducing E/I balance in CA1 pyramidal neurons.

Optogenetic Spike Trains Arrest New Spine Growth

Alterations in mPSC occurrence suggest changes in the density of synapses occurring through *de novo* formation or elimination of synapses. We have recently shown that inhibitory synapse formation, but not elimination, is increased during 24 hr following

spike trains leading to increased GABAergic synapse density in CA1 neurons (Flores et al., 2015). In order to determine whether the change in mEPSCs IEI arises from reduced excitatory synapse density, we analyzed the turnover of dendritic spines, which are structural proxies for excitatory synapses. Spines of ChR2-EYFP and mRFP co-transfected neurons were repeatedly imaged 5 and 24 hr after the stimulation using confocal microscopy, allowing longitudinal tracking of individual spines (Figure 2A). Blue light delivery caused a reduction in dendritic spine density after 24 hr in ChR2+ neurons (spike train), but not in mRFP-only expressing neurons (control light, Figures 2B and 2C). Spine density was unaffected in neurons expressing mRFP+ChR2 that received 670 nm, which does not activate ChR2 (control ChR2, Figure 2C). Spike trains did not alter the stability of spines present before stimulation (Figure 2D) or the fraction of lost spines (Figure 2E). However, spike trains decreased the growth of new dendritic spines 5 and 24 hr after the stimulation (Figure 2E). These results suggest that spike trains decrease excitatory synapse density by rapidly arresting the formation of new dendritic spines. Together with our previous results on GABAergic synapse plasticity (Flores et al., 2015), our data suggest that elevated optogenetically induced neuronal spiking of CA1 pyramidal neurons induces changes in synaptic density and currents (i.e., IPSCs and EPSCs) by rapid and differential regulation of inhibitory and excitatory synapse growth without affecting synapse elimination.

Mechanisms of Spike-Trains-Induced Arrest of New Spine Growth

We next characterized how spike trains induce changes in dendritic spine turnover in CA1 pyramidal neurons (Figure 3A). First, we applied spike trains and waited 48 hr or 4 or 5 days before assessing dendritic spine turnover (Figures 3A and 3B). Dendritic spine density and new spine formation returned to control values 4 or 5 days after spike trains but were still altered after 48 hr (Figures 3B–3D). To study the frequency dependency, we applied low-frequency spike trains (1 Hz instead of 10 Hz) and observed normal new spine growth and normal spine density (1 Hz; Figures 3C and 3D). The protein synthesis inhibitor anisomycin blocked the reduction in dendritic spine density and growth (anisomycin, Figures 3C and 3D). These results indicate that reduced dendritic spine turnover induced by optogenetically induced spike trains is reversible, frequency dependent, and requires protein synthesis. Interestingly, time-lapse confocal imaging of gephyrin-mCherry, a marker of inhibitory synapses (Flores et al., 2015), showed that *de novo* formation of GABAergic contacts increased 24 hr after spike trains and returned to control values 48 hr later (Figure S2), suggesting that spike-train-induced structural plasticity of inhibitory synapses is also reversible.

In order to test whether glutamatergic transmission and/or network activity are involved in homeostatic spine plasticity, we performed experiments in the presence of N-methyl-D-aspartate (NMDA), α -amino-3-hydroxy-5-methyl-4-isoxazole-propionic acid (AMPA) glutamate receptors antagonists, or voltage-dependent sodium channel blockers. None of the drugs tested prevented the reduction in new spine formation or spine density (D-AP5, NBQX, and tetrodotoxin; Figures 3E and 3F). This is in line with our recent findings that spike trains induced

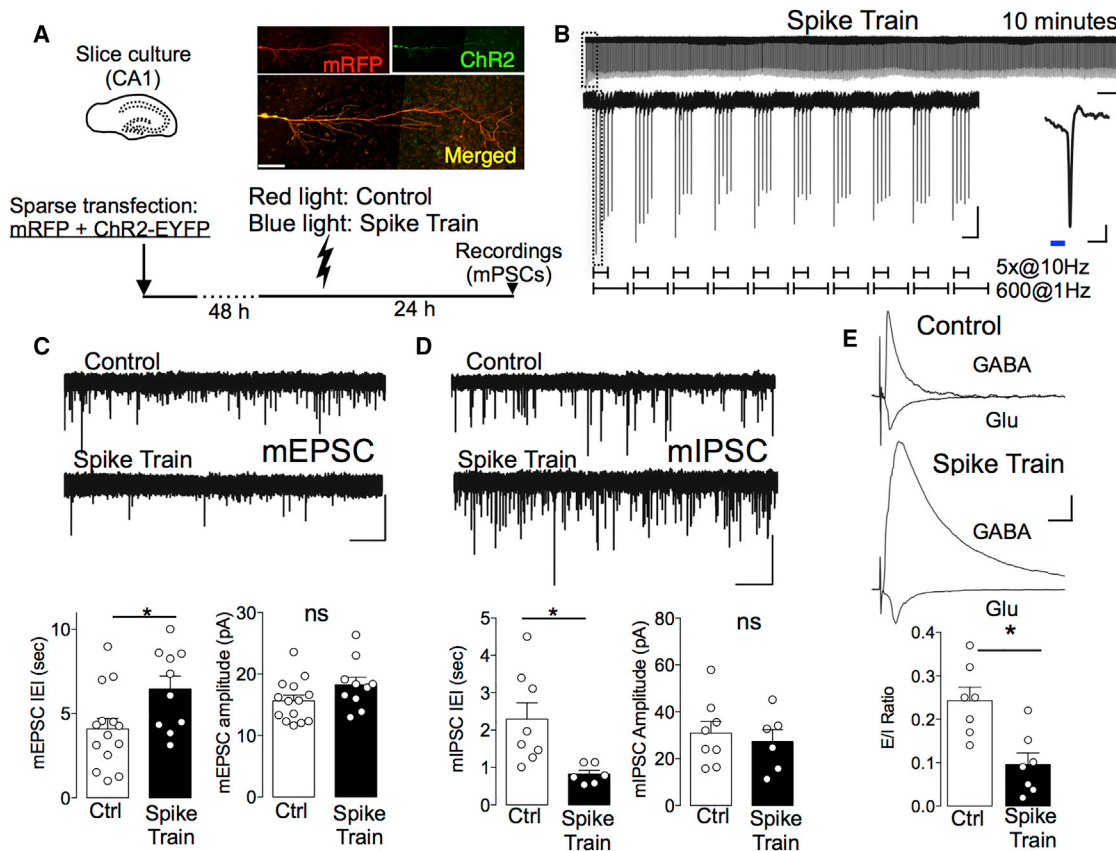


Figure 1. Optogenetically Induced Spike Trains Reduce Synaptic Excitability in CA1 Pyramidal Neurons

(A) Experimental protocol for the assessment of spike-train-induced homeostatic plasticity *in vitro*. Maximal projection composite image of two adjacent fields of view showing a cultured CA1 pyramidal neuron transfected with mRFP+ChR2-EYFP. The scale bar represents 50 μ m.

(B) Cell-attached recording during spike trains. Top trace shows the complete 10-min duration of spike trains. Action potentials (vertical deflections) were elicited by 5 pulses of blue light (blue lines, 20 ms) delivered at 10 Hz and repeated every second for 10 min. The middle trace shows the initial 50 and first light-induced action potential at an expanded timescale. The scale bars represent 30 s and 25 pA, 0.5 s and 75 pA, and 40 ms and 10 pA, respectively.

(C) Representative recordings in CA1 pyramidal neurons obtained 24 hr after stimulation. Vertical deflections are mEPSCs recorded in the presence of tetrodotoxin (TTX) (1 μ M) and GABA_A receptor blocker gabazine (SR95531; 10 μ M). The scale bar represents 25 pA and 20 s. Graphs are summary plots of frequency and amplitude of mEPSC. IEI: unpaired t test $t(22) = 2.43$; * $p = 0.02$; amplitude unpaired t test $t(22) = 1.70$; ns, non-significant; $p = 0.10$; $n = 14$; 10 recorded neurons.

(D) Same as in (B) but for inhibitory neurotransmission. mIPSCs were recorded in the presence of TTX (1 μ M) and AMPA receptor blocker (DNQX; 10 μ M). The scale bar represents 100 pA and 20 s. Graphs are summary plots of frequency and amplitudes of mIPSCs. IEI: unpaired t test $t(12) = 2.84$, * $p = 0.01$; amplitude unpaired t test $t(12) = 0.49$, ns, $p = 0.63$; $n = 8$; 6 recorded neurons.

(E) Electrically evoked excitatory and inhibitory postsynaptic currents (eEPSCs and eIPSCs) were simultaneously recorded 24 hr after spike trains by clamping membrane resting potential at -70 (glutamate) and 0 mV (GABA). The scale bar represents 200 pA and 25 ms. Graph is the summary plot of the ratio of the peak amplitudes of eEPSC and eIPSC. Unpaired t test $t(12) = 3.61$; * $p = 0.004$; $n = 7$ recorded neurons per group. Bars in graphs are mean \pm SEM; dots represent replicates.

See also Figure S1.

GABAergic synapse formation independently of the AMPA, NMDA receptors, and voltage-dependent sodium channel (Flores et al., 2015). Because homeostatic plasticity could be induced independently of network activity, we next tested the dependence on Ca^{2+} signaling. Blockade of dendritic L-type voltage-dependent Ca^{2+} channels (L-type VDCCs) using the selective blocker nifedipine completely blocked the effects of spike trains in dendritic spine turnover, preventing the decrease in spine density and formation (nifedipine, Figures 3E and 3F). Nifedipine did not change the probability or amplitude of optogenetically induced spikes, suggesting that L-type VDCC blockade

did not affect ChR2 function (Figure S3). These results show that optogenetically induced spike trains regulate dendritic spine turnover of CA1 pyramidal neurons through a mechanism that is independent of glutamate receptor and network activity but requires increase in intracellular Ca^{2+} levels through L-type VDCCs.

Spike Trains Induce Homeostatic Plasticity in Hippocampal Granule Cells *In Vivo*

We then turned to granule cells of the dentate gyrus. In preparation of the behavioral experiments, all manipulations were

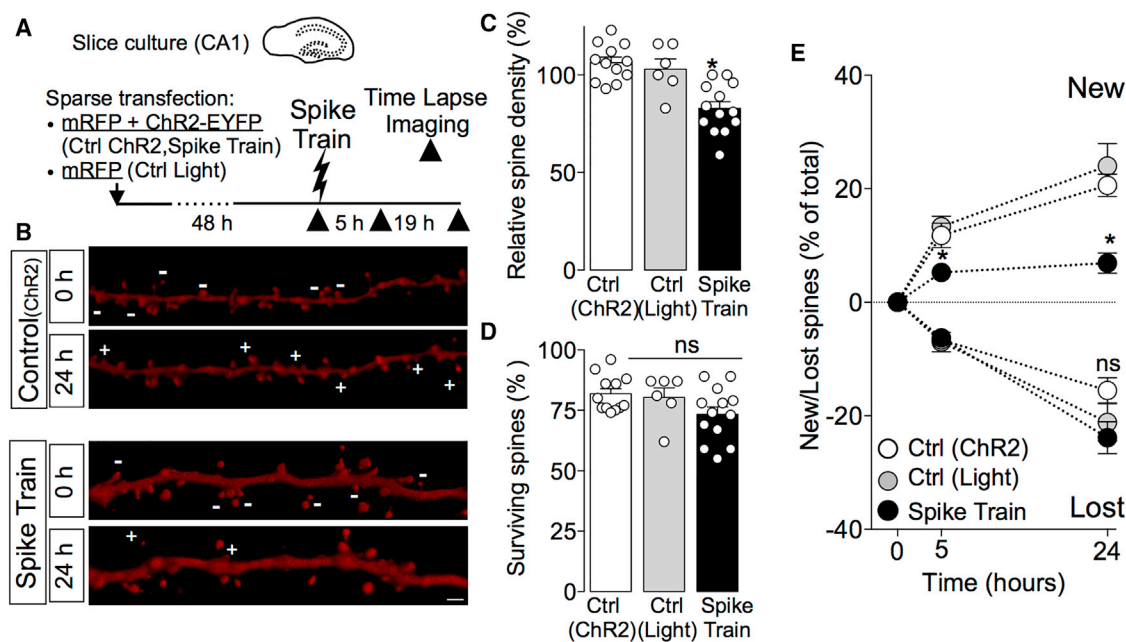


Figure 2. Optogenetically Induced Spike Trains Decrease Spine Density in CA1 Pyramidal Neurons by Arresting New Spine Formation

(A) Experimental protocol for time-lapse imaging of dendritic spines in cultured CA1 neurons. (B) Maximal projection images of dendritic segments imaged before and 24 hr after red (upper panel, control, ChR2) or blue (lower panel, spike train) light delivery. Minus and plus signs mark lost and new spines, respectively. The scale bar represents 2 μ m. (C) Optogenetically induced spike trains decreased spine density after 24 hr in mRFP+EYFP-ChR2, but not in control, neurons. One-way ANOVA $F(2,28) = 14.64$; $p < 0.0001$; * $p = 0.002$; $n = 12, 6,$ and 13 imaged neurons for Ctrl (ChR2), Ctrl (light), and spike trains, respectively. (D) No differences were observed in the stability of pre-existing spines. One-way ANOVA $F(2,28) = 2.69$; $p = 0.08$; $n = 12, 6,$ and 13 imaged neurons for Ctrl (ChR2), Ctrl (light), and spike trains, respectively. Bars in graphs (C) and (D) are mean \pm SEM; dots represent replicates. (E) Percentage of new and lost spines after spike trains. Note the decreased new spine growth already 5 hr after spike trains. New spines: two-way repeated-measures ANOVA $F(2,25) = 13.43$; $p = 0.0001$; * 5 hr, $p = 0.004$; 24 hr, * $p < 0.0001$. Lost spines: $F(2,25) = 1.12$; $p = 0.34$; ns; 5 hr, $p > 0.99$; 24 hr, $p = 0.34$; $n = 9, 6,$ and 12 neurons for Ctrl (ChR2), Ctrl (light), and spike trains, respectively.

carried out in granule cells *in vivo* because these neurons form context-specific ensembles that drive the recall of spatial memories (Liu et al., 2012). We expressed ChR2-mCherry in a low fraction of granule cells and induced spike trains in living mice using blue light delivered to the dentate gyrus through an optic fiber (Figure 4A). One group of animals was perfused 1 hr after spike trains delivery to assess the extent of neuronal activation using an immunostaining against the activity-regulated gene cFos. ChR2 was expressed in $12\% \pm 1\%$ of total granule cells revealed by DAPI staining (mean \pm SEM; $n = 10$ mice; Figure 4B), and high levels of cFos were detected in a majority of ChR2-expressing neurons after spike trains (spike trains $73\% \pm 7\%$, control $8\% \pm 2\%$; cFos+/ChR2+ neurons; unpaired t test $t(8) = 8.85$; $p < 0.001$; $n = 5$ mice per group; Figure 4C). Overall, optogenetically induced spike trains induced cFos expression in $9\% \pm 1\%$ of total granule cell population (mean \pm SEM; $n = 5$ mice).

Another group of animals was perfused 24 hr later, and synaptic changes were assessed in granule cells after spike trains delivered *in vivo*. We determined the density of excitatory and inhibitory synapses (visualized by adeno-associated virus [AAV]-mediated expression of GFP-tagged gephyrin) of stimulated granule cells using confocal microscopy (Figure 4D). We compared synapse density in ChR2-expressing neurons of control mice and mice that received *in vivo* spike train delivery 24 hr

before (Figure 4D). Spike trains increased the number of gephyrin-GFP clusters indicative of inhibitory synapses (control 0.9 ± 0.1 ; spike trains 1.3 ± 0.1 gephyrin spots/10 μ m; $p = 0.004$; Figure 4D) but reduced the density of dendritic spines located in the molecular layer of the dentate gyrus (control 1.1 ± 0.1 ; spike trains 0.83 ± 0.1 spine/ μ m; $p < 0.001$; Figure 4D). These results show that brief optogenetically induced spike trains decrease excitatory and increase inhibitory synapse density of granule cells *in vivo*.

Do functional changes accompany structural changes *in vivo*? To answer this question, eEPSC/eIPSC balance of stimulated neurons was assessed *ex vivo* in acute slices and compared with that of ChR2-expressing neurons of control mice, in which stimulation was performed with a blunted fiber that prevented blue light delivery (controls). Synaptic inputs were activated using an extracellular electrode consecutively placed in two different locations in the molecular layer of the dorsal dentate gyrus (Figure 4E). Increasingly long stimulus durations for each location were used in order to recruit a different set of presynaptic axons. The eEPSC/IPSC amplitude ratio for each stimulation intensity and each location was significantly lower in animals that had received spike trains as compared to control animals (Figure 4E). Nifedipine treatment (40 mg/kg; subcutaneous injection 30 min before spike trains) prevented the decrease in E/I ratio

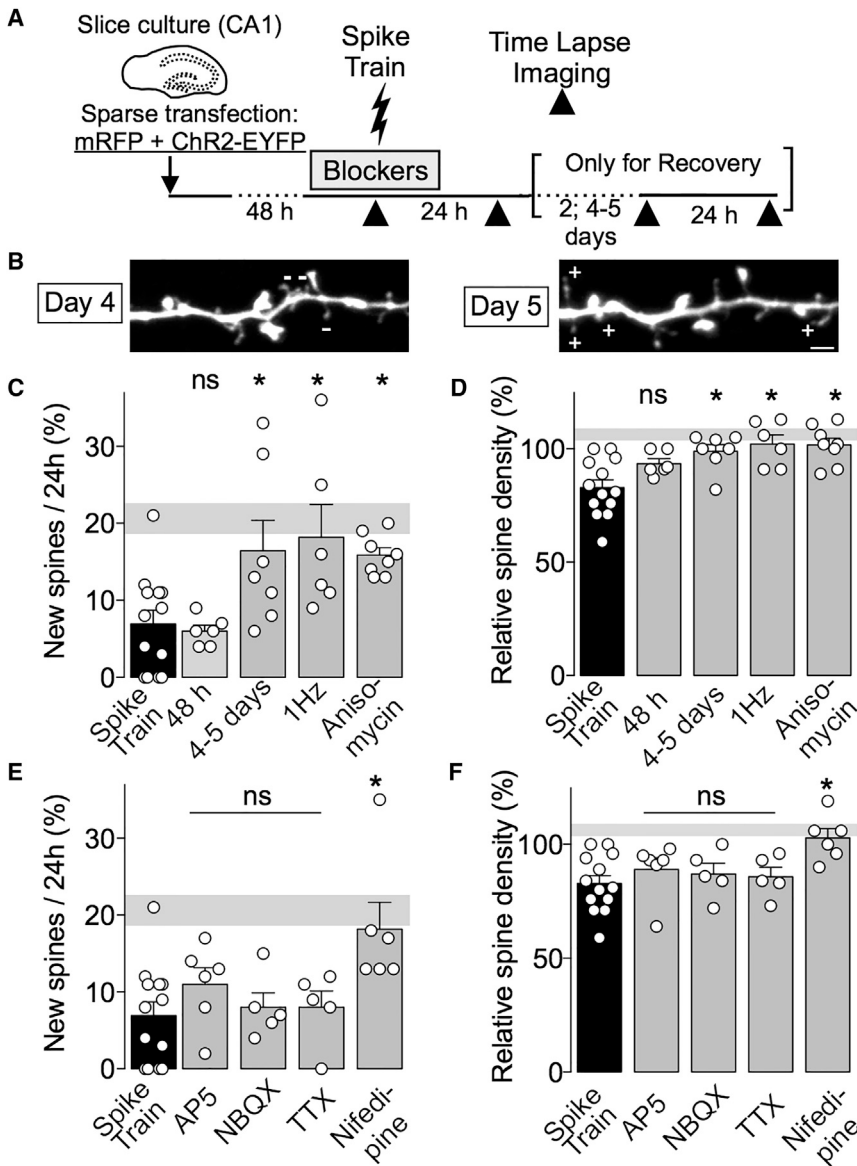


Figure 3. Mechanisms of Spiking-Induced Decrease in Spine Growth and Density

(A) Experimental protocol. Blockers (gray box) were applied 30–60 min before spike trains and washed out after 1 hr. Black bars in graphs (spike trains) represent values obtained in the immediate 24 hr after spike trains in untreated cultures. Grey shaded area corresponds to values (mean \pm SEM) of spine density and new spine growth in control unstimulated neurons.

(B) Representative images of dendritic segments obtained 4 and 5 days after spike train delivery. De novo spine formation (plus signs) occurs at the levels of non-stimulated neurons. The scale bar represents 2 μ m.

(C and D) 4 or 5 days, but not 48 hr, after spike trains, new spine formation (C) and density (D) returned to values similar to those of unstimulated CA1 neurons (gray shaded area). Low-frequency spike trains (1 Hz; 10 min) did not alter dendritic spine turnover (C) or density (D). Decreased density and reduced spine formation were abolished when spike trains were delivered in the presence of the protein synthesis inhibitor anisomycin (25 μ M), indicating protein synthesis dependency. One-way ANOVA, new spines: $F(4,35) = 5.15$, $p = 0.002$; * 4 or 5 days $p = 0.03$, $n = 7$; 1 Hz $p = 0.01$, $n = 6$; anisomycin $p = 0.04$, $n = 8$. One-way ANOVA, relative density: $F(4,35) = 6.83$, $p = 0.0004$; * recovery $p = 0.001$, $n = 8$ imaged neurons, 48 hr, ns, $n = 6$. (E and F) NMDAR blockade with DAP5 (10 μ M), AMPA receptor blockade with NBQX (10 μ M), or sodium channel blocker TTX (1 μ M) did not alter the effect of spike trains in dendritic spine formation (E) and density (F). However, L-type VDCC blocker nifedipine (20 μ M) prevented spike-train-induced decrease in dendritic spine density and growth. One-way ANOVA, new spines: $F(4,30) = 3.68$, $p = 0.01$; ns, AP5, NBQX, and TTX $p > 0.99$, $n = 6, 5$, and 5, respectively; nifedipine $p = 0.004$, $n = 6$. One-way ANOVA, relative density: $F(4,30) = 3.24$, $p = 0.02$; ns, AP5, NBQX, and TTX $p > 0.99$, $n = 6, 5$, and 5, respectively; nifedipine $p = 0.005$, $n = 6$ imaged neurons. Bars are mean \pm SEM; dots represent replicates.

See also Figures S2 and S3.

observed 24 hr after spike trains. These results suggest that optogenetically induced spike trains delivered *in vivo* decrease synaptic excitability of granule cells through an L-type-VDCC-mediated mechanism.

Spike Trains Regulate Memory Function of a Neuronal Ensemble

Coordinated activity of ensembles of granule cells in the dorsal hippocampus is essential for contextual fear memory (Liu et al., 2012; Denny et al., 2014). For this reason, we tested whether spike trains affect the memory function of granule cells. Because spike trains reduce synaptic excitability, we hypothesized that, when applied to the ensemble of neurons responsible for a contextual fear memory, spike trains may reduce the chance of coordinated reactivation and interfere with its mnemonic function.

We first tested the consequences of spike trains applied during training in the contextual fear conditioning protocol (CFC) on memory recall 24 hr later, when spike-trains-induced synaptic adaptations have taken place. Mice received spike trains during the training session of the CFC (Figure 5A). Conditioning was highly effective in control mice. These animals exhibited elevated freezing levels during the test session 24 hr after (Figure 5A, left panel) whereas, in contrast, freezing levels in mice where granule cells were optogenetically stimulated during conditioning were not enhanced (Figure 5A, middle panel). These results suggest an impaired ensemble activity during the recall session. In line with this interpretation, mice that received nifedipine treatment 30 min before training showed significant higher freezing levels during the test session (Figure 5A, right panel), yet overall freezing levels were reduced (control 39.8%, spike trains 8.2%, spike trains + Nif 17.3%, two-way ANOVA, $F(2, 25) = 4.575$,

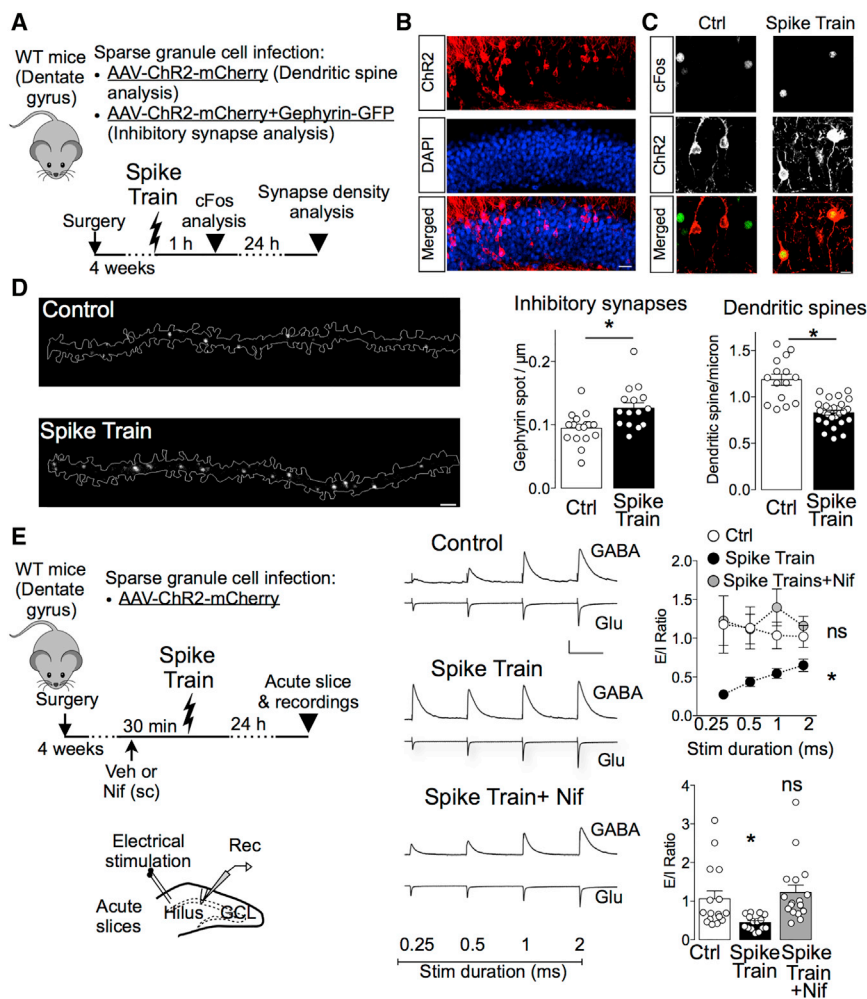


Figure 4. Optogenetically Induced Spike Trains Decrease Spine Density and Increase Inhibitory Synapse Number of Hippocampal Granule Cells *In Vivo*

(A) Experimental protocol for the assessment of spike-train-induced structural plasticity *in vivo*.

(B) Viral-mediated transduction of a sparse population of dentate granule cells. ChR2 (red) was expressed in $12\% \pm 1\%$ of total neurons revealed by DAPI (blue) staining. The scale bar represents 25 μm .

(C) Co-expression of cFos (green) and ChR2 (red) 1 hr after spike trains delivery to granule cells. cFos was detected in a majority of ChR2-expressing neurons after spike trains. The scale bar represents 10 μm .

(D) Representative images of ChR2-mCherry in dendrites of granule cells in spike trains and control mice. Dendrite profile showing dendritic spines was drawn using individual confocal planes. Gephyrin-GFP is shown as maximal projection image. Fluorescence outside the analyzed dendrite was omitted for clarity. Optogenetic stimulation decreased dendritic spine density but increased the number of gephyrin-GFP clusters in dentate granule cells. The scale bar represents 2 μm . Graphs: quantification of gephyrin-GFP cluster density in dentate granule cells, unpaired t test $t(31) = 3.11$, $^*p = 0.004$, $n = 16$ and 17 dendrites of 4 mice per group and dendritic spine density, Mann Whitney test, $U = 36$; $^*p < 0.001$, $n = 15$ and 17 dendrites from 3 or 4 mice per group.

(E) Experimental protocol for the assessment of spike-train-induced synaptic plasticity *in vivo*. The duration of the electrical pulse used to induce synaptic currents was progressively increased (0.25, 0.5, 1, and 2 ms) to recruit different sets of presynaptic terminals. Stimulation artifacts of the example traces were blunted for clarity. Graphs on the right are the summary plot of the ratio of the peak amplitudes of eEPSC and eIPSC for each

electrode location tested: top, two-way repeated-measures ANOVA, $F(2, 42) = 4.669$, $p = 0.015$, $^*p = 0.048$, $n = 15, 13$, and 17 stimulations per group from 8, 7, and 7 recorded neurons, bottom, Kruskal-Wallis test, $H = 18.38$, $p = 0.0001$; $^*p = 0.0094$, $n = 16, 15$, and 17 stimulations per group. The scale bar represents 100 pA and 250 ms.

Bars are mean \pm SEM; dots represent replicates.

$p = 0.02$; interaction $F(2, 25) = 13.62$, $p < 0.001$, C versus spike trains, $p = 0.02$; control versus spike trains +NIF, ns, $p = 0.14$; spike trains versus spike trains + Nif, ns, $p = 0.75$). As an additional control, nifedipine application 30 min before training in non-stimulated mice did not produce any changes in freezing levels during the test session (Figure S4A), indicating that nifedipine alone does not interfere with fear memory acquisition. These results suggest that L-type-VDCC-mediated synaptic adaptations caused by spike trains partially impair memory recall.

In a second experiment, spike trains were delivered selectively in neurons responsible for contextual fear memory (Figure 5B). To this extent, mice expressing the tamoxifen-inducible Cre recombinase under the control of the cFos promoter (cFosCreERT2 mice; Guenther et al., 2013) and wild-type (WT) littermates were injected in the dentate gyrus with AAVs expressing ChR2 in a Cre-dependent manner. One hour before the training session in the CFC paradigm, mice were injected

with 4-hydroxy-tamoxifen (Tam). This procedure induced sparse ChR2 expression specifically in granule cells activated during the behavioral paradigm only in cFosCreERT2 + mice, but not in WT (control) animals (Figure 5C), and did not affect the formation of short-term memory (Figure 5D; training). Three days after training, spike trains were delivered in the dentate gyrus during extinction training (exposition to the context without US; Figures 5B and 5D). During this session, both control and cFosCreERT2+ animals showed gradually diminishing levels of freezing, suggesting that both groups of animals equally learned to uncouple the CS and US (within session extinction; Figure 5D, extinction). Control mice showed elevated levels of freezing in the test session 24 hr during a brief re-exposure to the conditioning context, suggesting no extinction retention (Figure 5D, test). In contrast, cFosCreERT2+ mice that received spike trains in the conditioning context showed reduced freezing levels compared to WT littermates 24 hr later (Figure 5D, test). These results suggest that homeostatic synaptic adaptations induced by

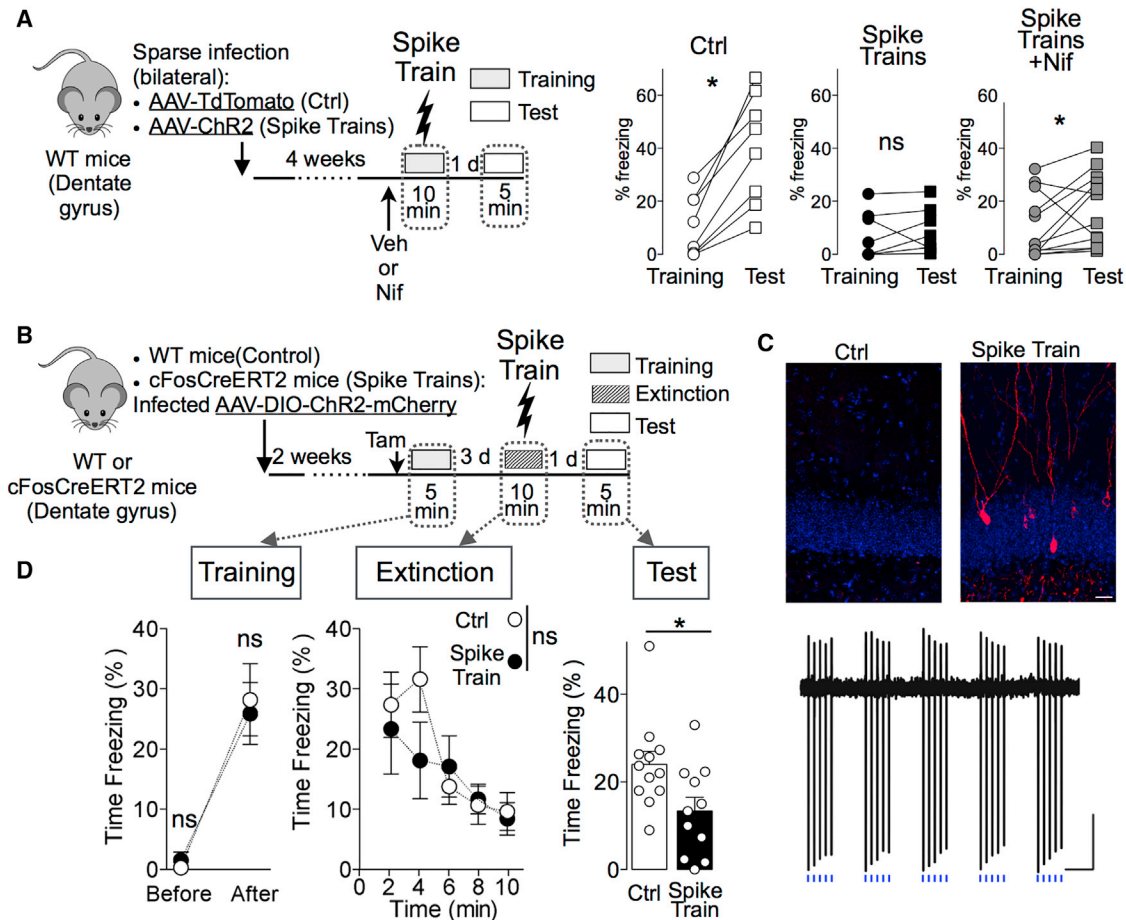


Figure 5. Optogenetically Induced Spike Trains in Dentate Granule Cells Regulate Memory Extinction

(A) Mice expressing tDTomato (Ctrl) or ChR2 expressing in a sparse population of hippocampal neurons were subcutaneous treated with nifedipine (Nif) or vehicle 30 min before training in the contextual fear conditioning protocol (gray box) with or without optogenetic stimulation (spike trains). One day later, fear memory recall was tested in the same context (white box). Graphs on the right show the percentage of time spent freezing during the complete training and recall sessions. Spike trains prevented training-induced freezing behavior in vehicle, but not in nifedipine-treated mice. Control, $t(7) = 5.881$, $p = 0.0003$; spike trains, $t(7) = 0.6489$, $p = 0.2686$; spike trains+Nif, $t(11) = 1.912$, $p = 0.0411$, one-tailed paired t tests; $n = 8, 8$, and 12 mice per group.

(B) A sparse population of granule cells active during contextual fear memory formation was tagged with ChR2 using mice expressing tamoxifen-inducible Cre recombinase under the control of cFos promoter (cFos-CreERT2 mice). Mice were trained in the contextual fear conditioning protocol (gray box) after 4-OH-tamoxifen (Tam) induction of Cre activity. Three days later, control stimulation (control; WT) and spike trains (spike trains; cFosCreERT2 mice) were delivered while mice were exposed to the conditioning context alone (extinction). Memory was tested 24 hr later by placing mice in the conditioning context (test).

(C) Expression of ChR2-mCherry (red) in a sparse population of dentate granule cells of cFosCreERT, but not control, mice after behavioral induction of the cFos promoter activity by contextual fear conditioning training. Images were obtained at the end of the experiment (4 days after induction) and counterstained with DAPI (blue) to reveal total cell population. The scale bar represents 25 μm . Trace below shows cell-attached *ex vivo* recordings of spike trains elicited by optical stimulation in neurons expressing ChR2 after contextual fear conditioning training. The scale bar represents 25 pA and 0.5 s.

(D) Quantification of conditioned response (time spent in freezing/total time) during the different steps of the behavioral protocol. Left graph (training): training induced similar levels of freezing in WT and cFosCreERT2 mice; two-way repeated-measures ANOVA $F(1,21) = 0.30$; $p = 0.58$; ns. Middle graph (extinction): freezing levels during extinction session are shown (mice were introduced in the conditioning context for 10 min without electric shocks). Freezing was quantified in 2-min epochs during spike train or control stimulation delivery; two-way repeated-measures ANOVA, $F(1,21) = 0.04$; $p = 0.83$; ns. Right graph (test): time mice spent freezing during the test session 24 hr after spike trains were delivered is shown; unpaired t test $t(21) = 2.46$; $p = 0.02$; $n = 12$ and 11 mice per group. Bars are mean \pm SEM; dots represent replicates. See also Figure S4.

optogenetically induced spike trains during recall facilitate long-term fear memory extinction.

Because extinction relies on the retrieval of a previously formed memory (Ouyang and Thomas, 2005), we next tested whether optogenetic stimulation of the neuronal ensemble is sufficient to induce memory extinction. To this extent, we applied

spike trains in a fear memory ensemble in anesthetized mice. Interestingly, freezing levels during the retention test of control and cFosCreERT2+ were undistinguishable when spike trains were delivered in anesthetized animals (Figure S4B). These results suggest that simultaneous fear memory recall is required for optogenetic facilitation of extinction.

DISCUSSION

Our experiments reveal that activity in the neural *ensemble* has long-lasting effects on synaptic function and impacts on fear memory performance. Pharmacological inhibition of the dorsal hippocampus with muscimol and optogenetic silencing of the dentate gyrus (DG) disrupts extinction, suggesting that neuronal activity in this brain area is required for memory extinction (Corcoran et al., 2005; Bernier et al., 2017). Our study is consistent with these studies and complements them by showing that enhanced neuronal activity in the DG engram may facilitate extinction of a contextual fear memory (without necessarily being sufficient). Because extinction requires the coordinated activity of distributed fear engram circuits (Maren, 2011), we cannot exclude an indirect effect. For example, optogenetic spike trains delivered to the DG may affect engram neurons in a connected brain area and trigger their homeostatic adaptations that affect memory extinction. Alternatively, the optogenetic spike trains may scramble circuit activity during training/extinction.

Regardless, the decreased synaptic excitability of the cellular engram may impair memory recall by reducing the reactivation of the engram during recall. Whereas this non-associative mechanism is an appealing model of how spike trains facilitate memory extinction, an associative neuronal process may also contribute (Myers and Davis, 2007). Homeostatic plasticity may create an inhibitory association among US and CS stimuli by lowering the excitatory connectivity and enhancing inhibitory interactions between the ensembles of neurons representing them. In this model, decreased synaptic excitability of the original cellular engram may reduce the weight of the initial fear context ensemble and favor the reinstatement of the memory trace formed during the extinction protocol. Because disinhibition controls fear memory formation in DG and amygdala (Stefanelli et al., 2016; Wolff et al., 2014), it is possible that dynamic regulation of E/I balance plays a role in the correct and adaptive expression of fear memories.

Extinction may reverse structural modifications induced by fear memory formation (Caroni et al., 2012). During context-shock association, synaptic potentiation and *de novo* formation of dendritic spines occurs in the ensemble of neurons defined by cFos expression in the dorsal DG (Ryan et al., 2015). Spike trains applied in this same ensemble trigger a decrease in spine density, similar to pharmacological and pathological models of amnesia that prevent memory recall (Ryan et al., 2015; Roy et al., 2016). A transient decrease in synaptic excitability may thus facilitate the disruption of the connectivity in the ensemble neurons specified during the conditioning process (Holtmaat and Caroni, 2016). Interestingly, homeostatic plasticity is not sufficient to facilitate extinction and require simultaneous memory recall because no effects are observed when optogenetically induced spike trains were delivered in anesthetized mice (Figure S4B). This is in line with the requirement of memory recall for behaviorally induced extinction that also relies on the retrieval of a previously formed memory (Ouyang and Thomas, 2005).

At the cellular level, optogenetic control of neuronal spiking in a fraction of hippocampal neurons *in vivo* or individual neurons *in vitro* induce compensatory synaptic adaptations. Our experiments confirm the cell-autonomous nature of homeostatic plas-

ticity (Goold and Nicoll, 2010). Neurons may individually sense their activity and react to prevent runaway excitation (Burrone et al., 2002). Our observations suggest a postsynaptic mechanism for the expression of homeostatic plasticity. However, a presynaptic mechanism via a retrograde messenger (Lourenço et al., 2014) cannot be formally excluded. Importantly, synaptic adaptations in CA1 pyramidal neurons were detected as early as 5 hr after spike trains and reverted to normal values 4 or 5 days after spike trains (Figures 3B, 3C, and S2). This form of plasticity of inhibitory and excitatory synapses is thus rapid and reversible, which makes it suitable to dynamically adapt synaptic input to ongoing levels of activity. Potential strategies to promote long-term effects on memory extinction include the use of chronic stimulation of the engram (Ramirez et al., 2015) or neuromodulatory strategies to enhance synaptic plasticity.

On the sub-cellular level, the primary parameter affected in excitatory and inhibitory transmission is synapse density. After the brief stimulation used in the current study (10 min), no changes in quantal amplitude of mEPSC were detected, likely because glutamate receptor internalization and synaptic depression require sustained (>12 hr) stimulation (Goold and Nicoll, 2010). Thus, similarly to experience-dependent plasticity, spike-trains-induced homeostatic plasticity relies on structural remodeling of hippocampal connectivity, protein synthesis, and intracellular Ca^{2+} levels. We confirm that Ca^{2+} influx through L-type VDCCs, but not NMDA receptors, is a main determinant of this form of plasticity (Goold and Nicoll, 2010). Prevention of spike-trains-induced memory impairment by *in vivo* nifedipine treatment was partial, suggesting that synaptic changes may not be blocked in a way that allows faithful reinstatement of specific spatio-temporal patterns of synaptic activity that occur during memory recall in control animals. We observed a convergence between the mechanisms of spike-trains-induced homeostatic plasticity and memory extinction. For example, previous studies have shown that L-type VDCCs facilitate contextual memory extinction (de Carvalho Myskiw et al., 2014). L-type VDCCs activated by synaptic spikes may thus trigger the activation of intracellular signaling pathways activated by and required for extinction (Fischer et al., 2007). In addition, L-type VDCCs are potent regulators of gene expression that may regulate somatic and dendritic synthesis of proteins. Newly synthesized proteins may be required for inhibitory synaptogenesis (i.e., gephyrin and Npas4) and dendritic spine pruning (i.e., group I mGluR and Arc/Arg3.1).

Back-propagating action potentials or dendritic spikes may act as potential sources of depolarization that trigger VDCC activity in physiological conditions (Sabatini and Svoboda, 2000). It is therefore possible that endogenous activity of hippocampal neurons has a similar effect on transmission and thus contributes to extinction. This is in line with the demonstration that neuronal activity in this range of frequency underlies spatial representations and memory recall (Liu et al., 2012). Optogenetic activation of a “safe” or “neutral” context during memory recall has been shown to reduce freezing levels in the conditioning context by activating a competing neural ensemble that interferes with the conditioning context spatial code (Garner et al., 2012). However, in our experiments, optogenetic activation of the fear engram during the extinction session did not significantly change

freezing levels (Figure 5D, extinction), suggesting that endogenous activity of engram cells in control mice is sufficient to induce high levels of freezing detected three days after conditioning. Our study suggests that modulation of neuronal activity may increase the efficiency of treatments to extinguish maladaptive memories in anxiety disorders. Spike trains elicited, for example, with transcranial magnetic stimulation could therefore be used to extinguish long-term fear memories that are prone to spontaneous recovery (Gräff et al., 2014).

To conclude, our results show that homeostatic plasticity induced through an optogenetic manipulation shapes functional and structural synaptic properties of a neuronal ensemble believed to represent the cellular engram. Further investigations will clarify how cell-autonomous and network-activity-dependent forms of synaptic plasticity interact to regulate memory function of neuronal ensembles. The current study provides a link between a specific form of synaptic plasticity and a cellular engram and may contribute to our understanding of post-trauma disorders that affect the neuronal substrates of extinction (Rothbaum and Davis, 2003).

EXPERIMENTAL PROCEDURES

Animals, Cell Culture, and Viral Vectors

Group-housed male and female adult (8–12 weeks) wild-type and cFosCreERT2 mice (B6.129(Cg)-Fos^{tm1.1(cre/ERT2)^{Luo}/J}) maintained in a 12-hr light/dark cycle and with unlimited access to food were used for the study. All mice lines were kept in a C57BL/6J genetic background. Hippocampal organotypic cultures are as previously described (De Roo et al., 2008b). Animal experimentation was performed according to protocols approved by the Institutional Animal Care and Use Committee of the University of Geneva and the Geneva Veterinary office.

AAVs used in this study were produced by the University of North Carolina and University of Pennsylvania vector cores. AAV-EF1a-DIO-hChR2(H134R)-mCherry (serotype 5) was co-injected with AAV-CamKII0.4-Cre (serotype 1; diluted 1:5,000) in order to obtain sparse optogenetic activation of hippocampal excitatory neurons. AAV-DIO-gephyrin-GFP (serotype 9) was constructed by introducing the Nhel-Smal fragment of a gephyrin-GFP fusion construct (Flores et al., 2015) in an emptied AAV vector backbone, driving Cre-dependent expression of gephyrin-GFP fusion under the control of the hSynapsin promoter.

Surgery and Transfection

Surgery was performed as previously described (Stefanelli et al., 2016). Briefly, analgesic-treated 8- to 12-week-old mice were anesthetized with 1.5%–2.0% isoflurane (w/v) and stereotaxic injections of 0.4 μ L viral vectors targeted to the dorsal DG (–2.2 anterior-posterior; \pm 1.4 medial-lateral; –1.9 dorsal-ventral). Custom-made optical fiber implants were positioned 0.5 mm above the DG. Dental cement darkened with charcoal powder was used to secure the implant and to prevent light efflux. Organotypic slice cultures were transfected at day in vitro 11 (DIV11) using a biolistic approach.

Optogenetic Stimulation

For *in vivo* optogenetic stimulation, fiber patch cords (0.39 numerical aperture [NA] 200 μ m core diameter; Thor Labs) were attached through a double rotary joint to the implanted fibers and a diode-pumped solid-state laser (DPSS) blue light laser (MBL-473/50 mW; CNI Lasers) used to deliver 20-ms pulses (calibrated output power of 6–8 mW). *In vitro* spike trains and control stimulations were performed placing transfected CA1 neurons (1 or 2 per organotypic slice culture) under the collimated light of an LED (diameter \approx 100 μ m) with red (625 nm) or blue (470 nm) light. Light pulses were of 20-ms duration with a nominal power at the exit of 0.790 and 0.653 mW for blue and red LEDs, respectively.

Nifedipine (40 mg/kg) was dissolved in 1:10 Kremphor solution and injected subcutaneously (5 mL/kg).

Confocal Imaging

Images were obtained in a confocal laser-scanning microscopy with a Fluoview 300 system (Olympus) or in Leica SP5 confocal microscope with a 20 \times /0.7 NA oil immersion or 40 \times /0.8 NA water immersion objective. 4–7 days after transfection, time-lapse confocal imaging and analysis of dendritic spines and inhibitory synapses were performed as described previously (Flores et al., 2015; De Roo et al., 2008a). Confocal microscopy of CA1 pyramidal neurons' dendrites in living animals and organotypic slice cultures shows comparable turnover rates of dendritic spines (De Roo et al., 2008a; Attardo et al., 2015). Analysis of activity-regulated cFos and gephyrin-GFP expression was performed in confocal images of brain slices containing the upper blade of the DG (0.4 \times 0.3 mm; \sim 2.5 pixel/ μ m; 4 μ m step size). Analysis was performed in at least three sections per animal.

Immunohistochemistry

Mice were injected with a lethal dose of pentobarbital (150 mg/kg) and perfused trans-cardiacally with cold PBS and 4% paraformaldehyde solution. Brains were extracted and submerged in fixative for 24 hr at 4°C. Immunostaining started by blocking 50- μ m-thick sections in PBS 10% BSA and 0.3% Triton X-100 followed by overnight incubation in PBS 3% BSA and 0.3% Triton X-100 with primary antibody: cFos (rabbit polyclonal; Synaptic Systems; Cat. number 226 003; 1:5,000). After 3 \times 15 min wash in PBST at room temperature, slices were incubated with 1:500 Alexa-conjugated secondary antibodies against the corresponding species (Alexa Fluor 488 and 555; Life Technologies). After 3 more steps of washing in PBST, slices were mounted and covered on microscope slides using mounting medium. DAPI containing mounting medium was used to estimate the fraction of hippocampal neurons infected in behavioral experiments.

Electrophysiology

Acute coronal brain slices containing dorsal hippocampus (300 μ m) were cut with a Leica vibratome in a solution containing 234 mM sucrose, 11 mM glucose, 26 mM NaHCO₃, 2.5 mM KCl, 1.25 mM NaH₂PO₄, 10 mM MgSO₄, and mM 0.5 CaCl₂ (equilibrated with 95% O₂–5% CO₂; 4°C). Recordings were obtained at room temperature from hippocampal neurons identified using fluorescence microscopy in oxygenated artificial cerebrospinal fluid: 126 mM NaCl; 26 mM NaHCO₂; 2.5 mM KCl; 1.25 mM NaH₂PO₄; 2 mM MgSO₄; 2 mM CaCl₂; and 10 mM glucose (pH 7.4). Intracellular solution for mPSC recordings contained 70 mM Kgluconate, 70 mM KCl, 2 mM NaCl, 2 mM MgCl₂, 10 mM HEPES, 1 mM EGTA, and 2 mM MgATP (pH 7.3) corrected with KOH (290 mOsm). Electrically evoked PSCs were measured with an intracellular solution composed of 125 mM CsMeSO₃, 2 mM CsCl, 10 mM HEPES, 5 mM EGTA, 2 mM MgCl₂, and 4 mM MgATP.

Signals were amplified using a Multiclamp 200B patch-clamp amplifier (Axon Instruments; Foster City, California, USA), sampled at 20 kHz, filtered at 10 kHz, and stored on a personal computer (PC). Data were analyzed using pClamp (Axon Instruments).

Fear Conditioning

Behavioral experiments were performed during the light period of the cycle. One week before the experiments, all animals were habituated to the experimenter by one or two daily sessions of 5 min handling. Contextual fear-conditioning chamber consisted in a 15 \times 18 cm methacrylate cage with a metallic grid floor scented with 0.5% ammoniac and covered with a black/white stripe pattern to produce additional contextual cues. Mice were placed in the cage and allowed 3 min exploration. Three mild electric shocks (0.5 mA; 2 s) were then delivered through the floor grid with 30-s interval. Mice stayed one additional minute before being returned to the home cage. Recall sessions (5 min) were performed in the same cage without electric shocks. Freezing behavior was monitored by video recordings that were digitized and automatically scored using Any-maze software (Stoelting, USA). A single intraperitoneal (i.p.) injection of 2 mg 4-OH-tamoxifen dissolved in 0.2 mL of corn oil was performed in CreERT2 mice and WT littermates 1 hr before the training in CFC.

Statistical Analysis

Two-tailed standard *t* tests were performed to compare Gaussian distributions, and Mann-Whitney tests were used for non-Gaussian distributions. 1- or 2-way ANOVA followed by Bonferroni post hoc tests were performed when indicated. Bars in the graphs represent mean \pm SEM. For all tests, we adopted an alpha level of 0.05 to assess statistical significance. Statistical analysis was performed using Prism (Graphpad software).

SUPPLEMENTAL INFORMATION

Supplemental Information includes four figures and can be found with this article online at <https://doi.org/10.1016/j.celrep.2018.01.025>.

ACKNOWLEDGMENTS

We dedicate this article to the memory of Dominique Muller. We thank Johannes Graff for the generous gift of cFosCreERT2 mice and Anthony Holtmaat for comments and discussion on the manuscript. This work was financed by Swiss National Science Foundation grant Sinergia and grant 310030B-144080 (D.M.) and SNF grant 310030-149985 (C.L.).

AUTHOR CONTRIBUTIONS

P.M. and D.M. conceived and designed the experiments. T.S., P.M., and C.E.F. performed the experiments and analyzed the data. P.M. and C.L. wrote the manuscript.

DECLARATION OF INTERESTS

The authors declare no competing interests.

Received: April 10, 2017

Revised: November 25, 2017

Accepted: January 9, 2018

Published: February 6, 2018

REFERENCES

- Abbott, L.F., and Nelson, S.B. (2000). Synaptic plasticity: taming the beast. *Nat. Neurosci.* *3*, 1178–1183.
- Attardo, A., Fitzgerald, J.E., and Schnitzer, M.J. (2015). Impermanence of dendritic spines in live adult CA1 hippocampus. *Nature* *523*, 592–596.
- Bernier, B.E., Lacagnina, A.F., Ayoub, A., Shue, F., Zelman, B.V., Krasne, F.B., and Drew, M.R. (2017). Dentate gyrus contributes to retrieval as well as encoding: evidence from context fear conditioning, recall, and extinction. *J. Neurosci.* *37*, 6359–6371.
- Bloodgood, B.L., Sharma, N., Browne, H.A., Trepman, A.Z., and Greenberg, M.E. (2013). The activity-dependent transcription factor NPAS4 regulates domain-specific inhibition. *Nature* *503*, 121–125.
- Burrone, J., O'Byrne, M., and Murthy, V.N. (2002). Multiple forms of synaptic plasticity triggered by selective suppression of activity in individual neurons. *Nature* *420*, 414–418.
- Caroni, P., Donato, F., and Muller, D. (2012). Structural plasticity upon learning: regulation and functions. *Nat. Rev. Neurosci.* *13*, 478–490.
- Corcoran, K.A., Desmond, T.J., Frey, K.A., and Maren, S. (2005). Hippocampal inactivation disrupts the acquisition and contextual encoding of fear extinction. *J. Neurosci.* *25*, 8978–8987.
- de Carvalho Myskiw, J., Furini, C.R., Benetti, F., and Izquierdo, I. (2014). Hippocampal molecular mechanisms involved in the enhancement of fear extinction caused by exposure to novelty. *Proc. Natl. Acad. Sci. USA* *111*, 4572–4577.
- De Roo, M., Klausner, P., Mendez, P., Poggio, L., and Muller, D. (2008a). Activity-dependent PSD formation and stabilization of newly formed spines in hippocampal slice cultures. *Cereb. Cortex* *18*, 151–161.
- De Roo, M., Klausner, P., and Muller, D. (2008b). LTP promotes a selective long-term stabilization and clustering of dendritic spines. *PLoS Biol.* *6*, e219.
- Denny, C.A., Kheirbek, M.A., Alba, E.L., Tanaka, K.F., Brachman, R.A., Laughman, K.B., Tomm, N.K., Turi, G.F., Losonczy, A., and Hen, R. (2014). Hippocampal memory traces are differentially modulated by experience, time, and adult neurogenesis. *Neuron* *83*, 189–201.
- Epsztein, J., Brecht, M., and Lee, A.K. (2011). Intracellular determinants of hippocampal CA1 place and silent cell activity in a novel environment. *Neuron* *70*, 109–120.
- Fischer, A., Radulovic, M., Schrick, C., Sananbenesi, F., Godovac-Zimmermann, J., and Radulovic, J. (2007). Hippocampal Mek/Erk signaling mediates extinction of contextual freezing behavior. *Neurobiol. Learn. Mem.* *87*, 149–158.
- Flores, C.E., Nikonenko, I., Mendez, P., Fritschy, J.M., Tyagarajan, S.K., and Muller, D. (2015). Activity-dependent inhibitory synapse remodeling through gephyrin phosphorylation. *Proc. Natl. Acad. Sci. USA* *112*, E65–E72.
- Garner, A.R., Rowland, D.C., Hwang, S.Y., Baumgaertel, K., Roth, B.L., Kentros, C., and Mayford, M. (2012). Generation of a synthetic memory trace. *Science* *335*, 1513–1516.
- Goold, C.P., and Nicoll, R.A. (2010). Single-cell optogenetic excitation drives homeostatic synaptic depression. *Neuron* *68*, 512–528.
- Gräff, J., Joseph, N.F., Horn, M.E., Samiei, A., Meng, J., Seo, J., Rei, D., Bero, A.W., Phan, T.X., Wagner, F., et al. (2014). Epigenetic priming of memory updating during reconsolidation to attenuate remote fear memories. *Cell* *156*, 261–276.
- Gruart, A., Muñoz, M.D., and Delgado-García, J.M. (2006). Involvement of the CA3-CA1 synapse in the acquisition of associative learning in behaving mice. *J. Neurosci.* *26*, 1077–1087.
- Grubb, M.S., and Burrone, J. (2010). Activity-dependent relocation of the axon initial segment fine-tunes neuronal excitability. *Nature* *465*, 1070–1074.
- Guenther, C.J., Miyamichi, K., Yang, H.H., Heller, H.C., and Luo, L. (2013). Permanent genetic access to transiently active neurons via TRAP: targeted recombination in active populations. *Neuron* *78*, 773–784.
- Harvey, C.D., Collman, F., Dombeck, D.A., and Tank, D.W. (2009). Intracellular dynamics of hippocampal place cells during virtual navigation. *Nature* *461*, 941–946.
- Hengen, K.B., Torrado Pacheco, A., McGregor, J.N., Van Hooser, S.D., and Turrigiano, G.G. (2016). Neuronal firing rate homeostasis is inhibited by sleep and promoted by wake. *Cell* *165*, 180–191.
- Herry, C., Ferraguti, F., Singewald, N., Letzkus, J.J., Ehrlich, I., and Lüthi, A. (2010). Neuronal circuits of fear extinction. *Eur. J. Neurosci.* *31*, 599–612.
- Holtmaat, A., and Caroni, P. (2016). Functional and structural underpinnings of neuronal assembly formation in learning. *Nat. Neurosci.* *19*, 1553–1562.
- Holtmaat, A., and Svoboda, K. (2009). Experience-dependent structural synaptic plasticity in the mammalian brain. *Nat. Rev. Neurosci.* *10*, 647–658.
- Josselyn, S.A., Köhler, S., and Frankland, P.W. (2015). Finding the engram. *Nat. Rev. Neurosci.* *16*, 521–534.
- Lai, C.S., Franke, T.F., and Gan, W.B. (2012). Opposite effects of fear conditioning and extinction on dendritic spine remodeling. *Nature* *483*, 87–91.
- Leutgeb, S., Leutgeb, J.K., Barnes, C.A., Moser, E.I., McNaughton, B.L., and Moser, M.B. (2005). Independent codes for spatial and episodic memory in hippocampal neuronal ensembles. *Science* *309*, 619–623.
- Liu, X., Ramirez, S., Pang, P.T., Puryear, C.B., Govindarajan, A., Deisseroth, K., and Tonegawa, S. (2012). Optogenetic stimulation of a hippocampal engram activates fear memory recall. *Nature* *484*, 381–385.
- Lourenço, J., Pacioni, S., Rebola, N., van Woerden, G.M., Marinelli, S., DiGregorio, D., and Bacci, A. (2014). Non-associative potentiation of perisomatic inhibition alters the temporal coding of neocortical layer 5 pyramidal neurons. *PLoS Biol.* *12*, e1001903.
- Maren, S. (2011). Seeking a spotless mind: extinction, deconsolidation, and erasure of fear memory. *Neuron* *70*, 830–845.

- Marsden, K.C., Shemesh, A., Bayer, K.U., and Carroll, R.C. (2010). Selective translocation of Ca²⁺/calmodulin protein kinase IIalpha (CaMKIIalpha) to inhibitory synapses. *Proc. Natl. Acad. Sci. USA* *107*, 20559–20564.
- Myers, K.M., and Davis, M. (2007). Mechanisms of fear extinction. *Mol. Psychiatry* *12*, 120–150.
- Nabavi, S., Fox, R., Proulx, C.D., Lin, J.Y., Tsien, R.Y., and Malinow, R. (2014). Engineering a memory with LTD and LTP. *Nature* *511*, 348–352.
- Ouyang, M., and Thomas, S.A. (2005). A requirement for memory retrieval during and after long-term extinction learning. *Proc. Natl. Acad. Sci. USA* *102*, 9347–9352.
- Petrini, E.M., Ravasenga, T., Hausrat, T.J., Iurilli, G., Olcese, U., Racine, V., Sibarita, J.B., Jacob, T.C., Moss, S.J., Benfenati, F., et al. (2014). Synaptic recruitment of gephyrin regulates surface GABA_A receptor dynamics for the expression of inhibitory LTP. *Nat. Commun.* *5*, 3921.
- Ramirez, S., Liu, X., MacDonald, C.J., Moffa, A., Zhou, J., Redondo, R.L., and Tonegawa, S. (2015). Activating positive memory engrams suppresses depression-like behaviour. *Nature* *522*, 335–339.
- Rothbaum, B.O., and Davis, M. (2003). Applying learning principles to the treatment of post-trauma reactions. *Ann. N Y Acad. Sci.* *1008*, 112–121.
- Roy, D.S., Arons, A., Mitchell, T.I., Pignatelli, M., Ryan, T.J., and Tonegawa, S. (2016). Memory retrieval by activating engram cells in mouse models of early Alzheimer's disease. *Nature* *531*, 508–512.
- Ryan, T.J., Roy, D.S., Pignatelli, M., Arons, A., and Tonegawa, S. (2015). Memory. Engram cells retain memory under retrograde amnesia. *Science* *348*, 1007–1013.
- Sabatini, B.L., and Svoboda, K. (2000). Analysis of calcium channels in single spines using optical fluctuation analysis. *Nature* *408*, 589–593.
- Stefanelli, T., Bertolini, C., Lüscher, C., Müller, D., and Mendez, P. (2016). Hippocampal somatostatin interneurons control the size of neuronal memory ensembles. *Neuron* *89*, 1074–1085.
- Tonegawa, S., Liu, X., Ramirez, S., and Redondo, R. (2015). Memory engram cells have come of age. *Neuron* *87*, 918–931.
- Turrigiano, G.G., and Nelson, S.B. (2004). Homeostatic plasticity in the developing nervous system. *Nat. Rev. Neurosci.* *5*, 97–107.
- van Versendaal, D., Rajendran, R., Saiepour, M.H., Klooster, J., Smit-Rigter, L., Sommeijer, J.P., De Zeeuw, C.I., Hofer, S.B., Heimel, J.A., and Levelt, C.N. (2012). Elimination of inhibitory synapses is a major component of adult ocular dominance plasticity. *Neuron* *74*, 374–383.
- Vitureira, N., Letellier, M., and Goda, Y. (2012). Homeostatic synaptic plasticity: from single synapses to neural circuits. *Curr. Opin. Neurobiol.* *22*, 516–521.
- Wolff, S.B., Gründemann, J., Tovote, P., Krabbe, S., Jacobson, G.A., Müller, C., Herry, C., Ehrlich, I., Friedrich, R.W., Letzkus, J.J., and Lüscher, A. (2014). Amygdala interneuron subtypes control fear learning through disinhibition. *Nature* *509*, 453–458.
- Zuo, Y., Yang, G., Kwon, E., and Gan, W.B. (2005). Long-term sensory deprivation prevents dendritic spine loss in primary somatosensory cortex. *Nature* *436*, 261–265.